Geometric rules for the annihilation dynamics of step lines on fracture fronts

Will Steinhardt[1,2] and Shmuel M. Rubinstein[3]

[1]*Department of Earth and Planetary Sciences, Harvard University, Cambridge, Massachusetts, 02138, USA*

[2]*Department of Earth and Planetary Sciences, University of California Santa Cruz, Santa Cruz, California 95064, USA*

[3]*The Racah Institute of Physics, Hebrew University, Jerusalem, Israel, 91904*

(Received 30 November 2022; accepted 4 April 2023; published 9 May 2023)

The roughness of a fracture surface records a crack's complex path through a material and can affect the resultant frictional or fluid transport properties of the broken medium. For brittle fractures, some of the most prominent surface features are long, step-like discontinuities called step lines. In heterogeneous materials, the mean crack surface roughness created by these step lines is well captured by a simple, one-dimensional ballistic annihilation model, which assumes the creation of these steps is a random processes with a single probability that depends on the heterogeneity of the material, and that their destruction occurs via pairwise interactions. Here, through an exhaustive study of experimentally generated crack surfaces in brittle hydrogels, we examine step interactions and show that interaction outcomes depend on the geometry of the incoming steps. The rules that govern step interactions can be categorized into three unique classes and are fully described, providing a complete framework for predicting fracture roughness.

DOI: 10.1103/PhysRevE.107.055003

I. INTRODUCTION

Most materials have rough fracture surfaces. These surfaces form dynamically in the wake of a propagating crack front, with their roughness reflecting the complexity of the fracture's path. Crack roughness can affect both the dynamics of fracture [1], as well as the resultant fluid transport [2–4] or frictional properties [5–10] of the broken material.

While many brittle crack surfaces appear largely flat and smooth, a close inspection of both hard [11–13] and soft [14–19] materials reveals the presence of long, step-like discontinuities known as step lines. Step lines form during crack propagation as the front experiences a critical twist, or mixed mode I + III loading (opening + out-of-plane shear, respectively) [11,12,18,20–29], and in response nucleates a step that begins to grow in height. As the crack propagates, this step leaves an elongate scar on the fracture surface known as a step line, which acts as a topographic boundary separating two nominally flat surfaces onto distinct planes [11,12,20,22,23,30–33]. The twisting required to generate these steps can result from applied boundary conditions [11,12,20,22,23,30] or, under homogeneous confining stress, can arise from interactions between the front and local material heterogeneity [31–33].

For real, heterogeneous materials, it had been assumed that their rough crack surfaces resulted from complex fracture behavior that was highly sensitive to the specific details of the medium, and thus was difficult to accurately model. However, recent work has shown that crack roughness in heterogeneous materials can be well captured by a simple framework that is broadly insensitive to the specifics of a material [33]. For materials with well-distributed inhomogeneity, steps form at a constant probability when the propagating front interacts with the stress field surrounding localized heterogeneity. After forming, step lines drift laterally along the front in either direction at a rate equal to crack propagation, forcing them to interact with one another in a manner that on average reduces the number of steps. This process is well modeled by ballistic annihilation kinetics, which produce a reduction in the number of steps that grows as $\sim\sqrt{\text{time}}$ [34]. These opposing forces, step creation and annihilation through interaction, eventually balance and the fracture front reaches a steady-state number of steps and, thus, produces a steady-state roughness that is exclusively a function of the probability of step nucleation. This basic framework for the evolution of brittle fracture fronts can be used to predict the resultant crack roughness based on the heterogeneity present. However, it assumes that interactions are random and of a single, point-like nature, while previous work showed that steps can have both point-like and elongated interactions depending on the geometry of the incoming steps [16].

Through the analysis of three-dimensional crack surface topography measured in brittle hydrogels, we show that step interactions are highly deterministic. Steps have a characteristic asymmetric shape, which provides a constraint that fully defines both their direction of motion and their interactions with other steps. Since a step is bound to a crack front, it can have only four possible orientations, implying sixteen possible interactions. However, due to symmetry, there are only four unique interactions, which can be categorized into three classes. These interactions follow straightforward rules that can predict the resultant outgoing steps based exclusively on the orientations and sizes of the incoming steps. These rules provide a complete framework for accurately predicting three-dimensional crack roughness.

II. METHODS

$1 \times 1 \times 1$ inch^3 brittle hydrogel cubes are prepared and fractured by flowing a dyed fluid into a small prefracture that grows to generate a large flat crack surface, as seen in

 ©2023 American Physical Society

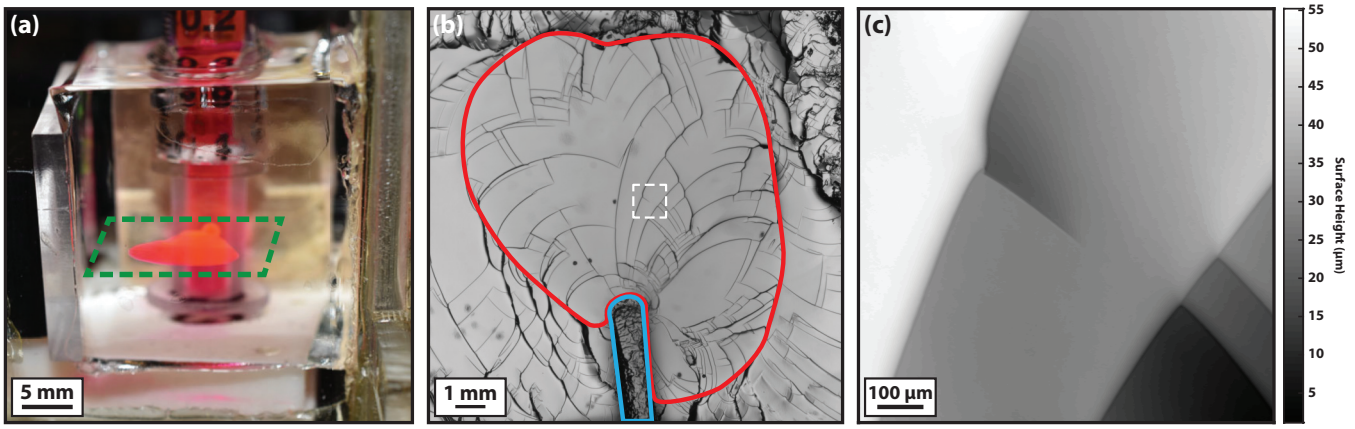

FIG. 1. (a) Example of a typical fracture experiment. A predominantly planar hydraulic fracture filled with a dyed, index-matched fluid that is allowed to diffuse into the hydrogel after crack propagation is ceased. Dashed green box represent the approximate surface in the middle panel. (b) Bright-field microscopy image of a fracture surface showing an abundance of step lines and interactions. The interior of the large red circle represents the area fractured hydraulically during the experiment, while the exterior is broken by hand after the experiment to expose the surface for imaging. Lower blue region shows the prefracture where the crack begins and propagates approximately radially. White dashed-line is the region shown in the right panel. (c) Topographic surface of the hydrogel with multiple step interactions measured via confocal microscopy. Crack propagates approximately from bottom to top.

Fig. 1(a). The methods for hydrogel preparation and fracture were previously described in detail by Steinhardt and Rubinstein [33]. This previous work also showed that the addition of glycerol to the solvent before polymerization consistently generates an increasing density of step lines. The inhomogeneity that leads to the formation of these step lines is likely due to one of many possible mechanisms that cause structural heterogeneity in hydrogels [35] being accentuated by the presence of a second phase in the solvent. An advantage of generating heterogeneity in this manner is that the gels remain fully transparent, allowing the resultant crack topography to be measured via confocal microscopy. For the majority of these experiments gels were polymerized at a glycerol concentration that would generate a moderate density of steps (≈40% vol), leading to interactions that were both frequent but also far from other steps, as seen for a typical surface in Fig. 1(b). The hydrogels utilized were measured through standard three-point bending tests and have the following properties: $E \approx 100$ kPa, $K_{IC} \approx 1000$ Pa$\sqrt{\text{m}}$, and $\Gamma \approx 10$ J/m^2, where E is the Young's modulus, K_{IC} is the plane strain fracture toughness, and Γ is the fracture energy.

The samples are hydraulically fractured with a fluorescent-dyed and index-matched fracturing fluid made from a mixture of water and dimethyl sulfoxide (DMSO) that has a viscosity close to that of water (max. 3.72 cP). After the gel has been fractured, the fluorescent dye in the fracturing fluid is allowed to diffuse into the hydrogel for approximately 5 minutes. The two sections of the gel are then fully separated by hand and postmortem regions are imaged on a bright-field microscope to create a map of the fracture surface. Localized $\approx 1 \times 1$ mm^2 regions are imaged with a confocal microscope at a resolution of $1.7 \times 1.7 \times 0.1$ µm^3, as seen in Fig. 1(c). The resulting scans are postprocessed into a height map, which is tilt corrected and characterized through a combination of image processing and hand measurements. A typical surface and corresponding height maps of different interactions is shown in Fig. 2.

Postmortem surfaces do not locally carry explicit information of the front's location in time. Nevertheless, the crack front and propagation direction can be deduced from a combination of (i) the known nucleation point and final extent of the fracture, (ii) the knowledge that step lines maintain a

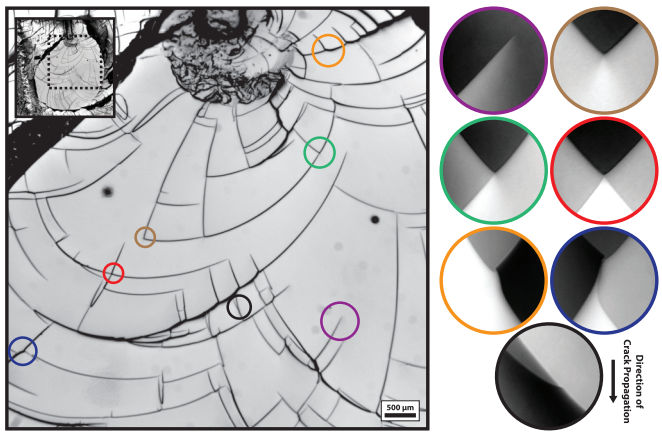

FIG. 2. A typical fracture surface with height maps of the different types of step interactions. (left) Bright-field microscope image of portion of a typical fracture surface (full surface with this region highlighted by dashed black square inset). The surface is pervasively covered by step lines that drift and interact. Each unique type of interaction is highlighted by a colored circle. (right) Height maps of the corresponding regions measured by confocal microscopy show the unique morphology of step interactions. Grayscale corresponds linearly to a height range from 0 to 20 µm (black to white) for each surface besides the third row (blue and orange), which go from 0 to 30 µm. The area of each image scales according to the size of the corresponding circle on the left image. Each map has been reoriented so that the crack propagation direction is top to bottom.

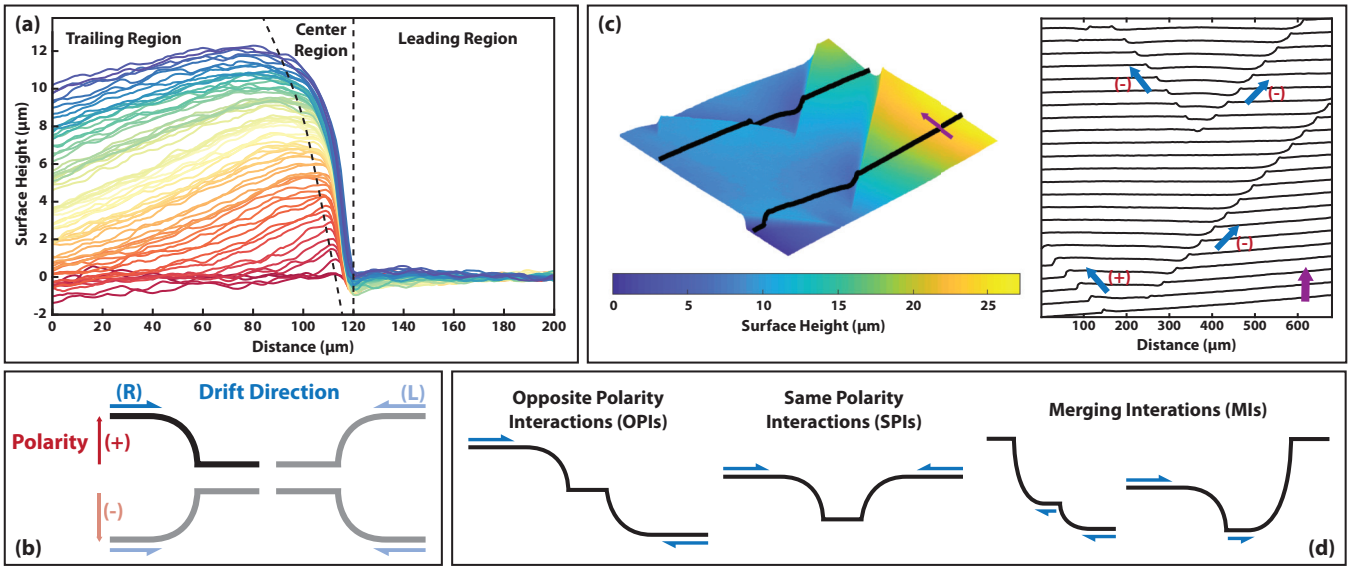

FIG. 3. Steps are asymmetric with a shape that defines their motion and interaction. (a) Cross sections of a single growing step aligned with their minimum values at $x = 120$ and an average of their 40 rightmost values at $y = 0$. Color represents the distance along the step. Aligning the steps in this manner reveals three distinct regions to a step: A flat "leading region" ending in a cusp, a steep "center region" that extends from the cusp to the peak which accounts for most of the relief and is slightly convex in the direction of drift, and a "trailing region" that extends away from the peak and changes from concave to nearly flat as the step grows. (b) A schematic diagram of a step showing that there are exactly four possible orientations for a single step on a given fracture front. (c) (left) Topography of a typical fracture surface containing five steps with two topographic cross sections shown in black. (right) Evenly spaced cross sections of the same surface separated vertically to give a sense of dynamics. Steps can have a positive (+) or negative (−) polarity (red), and drift in a direction (L or R) defined by their asymmetric shape (blue). (d) Schematic diagrams of step interactions. Since steps are bound to the same front, and their shape defines the direction of drift along the front, due to symmetry there are only three *unique* classes of possible step interactions.

45° angle to the crack front [16,18], and (iii) the fact that the fracture front can only move through unbroken material. While horizontal cross sections do not perfectly reflect the complex shape of the crack front, they allow consistent and comparable evaluations of the shape and size of steps from which the rules that govern interactions can be understood.

While the crack front is curved, complex, and does not move at a constant speed across the entire front, for the localized regions discussed below, horizontal cross sections allow consistent and comparable descriptions of the shapes and sizes of steps from which the rules that govern steps and their interactions can be understood.

III. STEP MORPHOLOGY

When a step initially forms it has three distinct regions: (1) a flat region that ends at a cusp, (2) a nearly vertical region that extends from the cusp to the peak, and (3) a decaying region that extends away from the peak, as shown in Fig. 3(a). We refer to these regions as the leading region, the center region, and the trailing region, respectively. As the step grows, the leading region remains static, the center region grows to a steady-state height, H_s (see Fig. 4), while the trailing region grows laterally, subtly reorienting until eventually the entire trailing region is horizontal.

Upon nucleation, steps quickly grow toward H_s, and surprisingly, steps that become larger than H_s due to additive step interactions, shrink back towards it (see the Supplemental Material [36]). For the composition of hydrogels used in this work, $H_s \approx 8$–10 μm and is largely invariant to the size of the perturbation caused by heterogeneity in the system; however, H_s does decrease with increased cross-linker (see the Supplemental Material [36]). Increasing the cross-link density is generally associated with an increase in

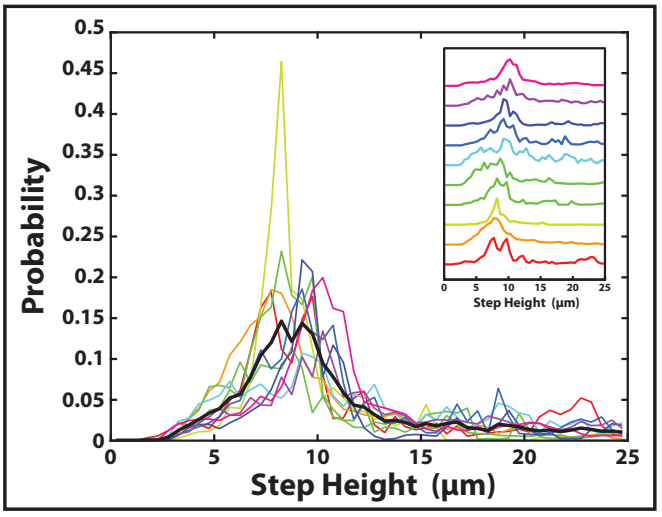

FIG. 4. Histograms of step heights measured from 10 different confocal scans across hydrogels with identical material compositions and fracturing procedures. Color (red to magenta) indicates the order of the measured steady-state heights (histogram peaks) from lowest to highest. Black line indicates the average of all surfaces. (Inset) The same data rescaled and distributed vertically with increasing steady-state height from bottom to top.

Young's modulus E and a decrease in fracture energy Γ for hydrogels [37,38]. Thus, the decrease in H_s is consistent with previous work showing that step heights are related to the characteristic length scale Γ/E [14].

The fractures in this study are penny-shaped cracks, thus it is useful to describe them with cylindrical coordinates, where the crack propagates in the r direction in the r-θ plane, and has a thickness in the z direction. A cartoon of a generic step that has reached its steady-state height is shown in the top-left corner of Fig. 3(b). Two disparate planes bound the interaction on either side, and thus we refer to them as the bounding planes. In addition, the step is asymmetric, due to the curvature of the center region and the fact that one part of the center region ends in a sharp cusp, while the other does not. For a horizontal fracture plane, this geometry has four potential orientations, as shown in Fig. 3(b). As the fracture propagates, the steps drift along the front in the θ direction, either left or right. The rate of drift is identical to fracture speed, so the lines maintain a constant angle to the front, or front angle, of 45° [16,18]. Steps are fully characterized by their height, drift direction along the front, and polarity, which is either positive or negative and which indicates whether the curved, center region is above (+) or below (−) the flat, leading region. We observe that the orientation of a step explicitly defines its drift direction as well as how it will interact with other steps, as seen in Fig. 3(c). While the precise morphology of step lines has been debated, these measurements agree with the many accepted features common to all previous descriptions: Steps are asymmetric with a flat region and a curved region that meet at a single point, and the orientation of that asymmetry sets the direction of motion along the front [12,14–16,18,20].

Steps reside on the fracture front and are thus bound to the same line. As a result, the drifting steps cannot circumvent one another and instead must interact [16,33]. Through our analysis we identify the rules of step line interactions. Steps that drift away from one another do not interact. Steps that drift towards one another must interact, with two unique classes of interactions: Same polarity interactions (SPIs), which are point-like, and opposite polarity interactions (OPIs), which are elongated. Even steps drifting in the same direction will occasionally attract, with one step accelerating towards the other until they merge. We refer to these as merging interactions (MIs). A cartoon of each type of interaction is shown in Fig. 3(d). Each class of interaction follows an algorithmic set of rules, where for every event the incoming steps can be used to predict or constrain the resultant outgoing steps. The complete rules that govern these interactions are detailed below.

IV. SAME POLARITY INTERACTIONS

All same polarity interactions (SPIs) begin with two incoming steps of the same polarity that approach one another from the left and right, with front angles of $+45°$ and $-45°$, respectively. These steps meet at a single point and their interaction has three distinct potential outcomes: Zero, one, or two outgoing steps. Due to their shape when viewed from above, these interactions are referred to as V, Y, and X interactions, respectively, as shown for four typical examples in Fig. 5(a). In each case, all outgoing steps have the same polarity as the incoming steps. For consistency, all the data has been reoriented such that the incoming steps are + steps.

The most commonly observed type of SPI is the Y interaction. The difference in height between the incoming steps, $\Delta H^{IN} = H_R^{IN} - H_L^{IN}$, determines the outgoing step, as shown in Fig. 5(b). Outside of a region where $\Delta H^{IN} \approx 0$, the shape and drift direction of the outgoing step is the same as that of the larger incoming step.

Y interactions can occur for both small and large $|\Delta H^{IN}|$ but behave differently in each case. For large $|\Delta H^{IN}|$, the step heights subtract, resulting in a single step with a height of $\approx|\Delta H^{IN}|$ that spans the bounding planes, as shown in Fig. 5(a). The removal of the middle plane and connection of the bounding planes with a single, smaller step, reduces the total length of the front, consistent with a process that minimizes energy. For small $|\Delta H^{IN}|$ the dynamics are different. Here, as the steps meet they merge and nearly annihilate, initially reducing the length of the front. However, this lower energy state does not persist, and instead, a single new step emerges above the bounding planes, increasing the overall front length, as seen in Fig. 5(a).

X and V interactions predominantly occur for small values of $|\Delta H^{IN}|$, as shown in Fig. 5(c). For both classes of interaction, the incoming steps meet, and nearly merge, in an identical manner to small-$|\Delta H^{IN}|$ Y interactions. The outgoing steps in X interactions behave similarly to small-$|\Delta H^{IN}|$ Y interactions, with two divergent steps (rather than one) forming and growing above the bounding planes, as shown in Fig. 5(a). For V interactions, instead of a step, a smooth, stepless hump is formed that eventually flattens out to a plane, as shown in Fig. 5(a). V interactions are the rarest interactions, with many fracture surfaces having none. V interactions also occur for an even narrower range of $|\Delta H^{IN}|$ around zero. Notably, there exists a similar range of small $|\Delta H^{IN}|$ values over which X, V and Y interactions all occur. These interactions are indistinguishable up to the point where they interact and nearly merge, and yet, they have markedly different outcomes, indicating that the type of interaction is not determined exclusively by step height.

The geometry of SPIs dictates that the height of one or both incoming steps must be larger than the difference in height of the bounding planes. This allows a straightforward means of reducing the total front length by connecting the bounding planes with a smaller step. By contrast, for OPIs the difference in height of the bounding planes is always, by definition, larger than either individual step. As a result, OPIs have more complex morphology.

V. OPPOSITE POLARITY INTERACTIONS

In many ways, opposite polarity interactions (OPIs) appear to be similar to X and Y SPIs: All OPIs have symmetrically identical inputs with two incoming steps and one or two outgoing steps, all of which have front angles of $\pm45°$. However, every OPIs has an additional intermediate region containing a single, middle step that connects the incoming and outgoing parts of the interaction, as shown for two typical examples in Fig. 6(a).

For OPIs, the incoming steps always drift towards one another with a front angle of $\pm45°$. These steps meet and form

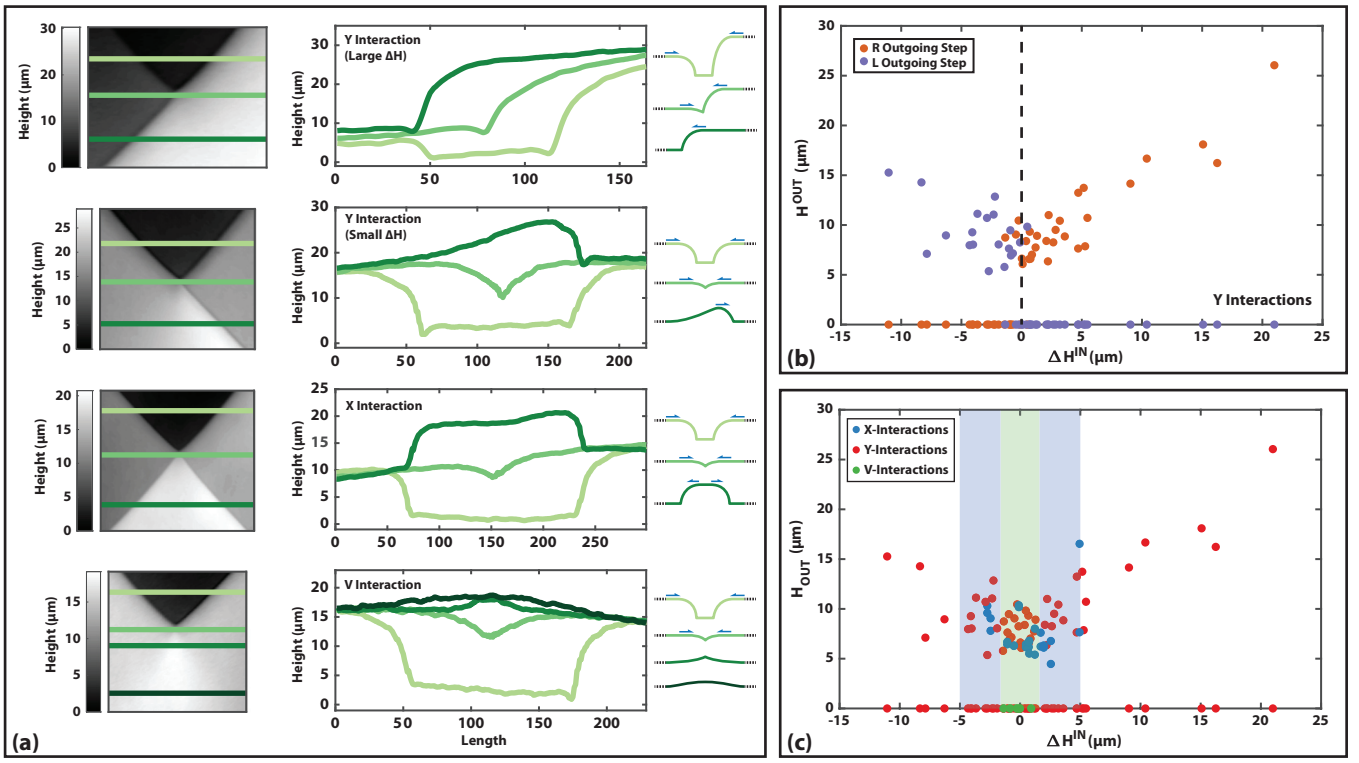

FIG. 5. An overview of same polarity interactions (SPIs). (a) Height maps (left), cross sections (middle), and schematics (right) of the four types of SPIs: Large-$|\Delta H^{IN}|$ Y interactions, small-$|\Delta H^{IN}|$ Y interactions, X interactions, and V interactions (top to bottom). Each height map is oriented so that the direction of crack propagation is from top to bottom. (b) Plot of the outgoing step height as a function of $\Delta H^{IN} = H_R^{IN} - H_L^{IN}$ for all Y interactions. Whether the resultant outgoing step travels right (orange) or left (purple) is determined by which incoming step is larger as indicated by the sign of ΔH^{IN}. (c) The same plot for all types of SPIs shows that X interactions only occur for $|\Delta H^{IN}| < 5$ μm (outer blue shaded region), and V interactions only occur for if the incoming step heights are nearly identical ($|\Delta H^{IN}| < 2$ μm, central green shaded region). However, the incoming step heights are not deterministic of the type of interaction as X, Y, and V interactions all occur over a similar range of $|\Delta H^{IN}|$.

a single middle step that connects the bounding planes, whose height is thus the sum of the heights of the incoming steps. Similar to SPIs, the middle step of an OPI has the shape and polarity of the larger of the incoming step, which we refer to as the "winning" step, as shown in Fig. 6(b). This step also has an increased front angle of approximately ±75°. The larger (or only) of the outgoing steps is a continuation of the middle step, retaining its, and thus the winning step's, polarity and drift direction. The other outgoing step (if one is present), which we refer to as the "losing" step, always drifts in the opposite direction, and can have either a positive or negative polarity, with both outgoing steps quickly returning to a front angle of ±45°.

While SPIs are point-like, with the incoming and outgoing steps appearing to sit on the same line in the r-θ plane, due to the presence of the middle step, OPIs are elongate interactions. This shifts the pairs of incoming and outgoing steps that drift in the same direction relative to each other by an offset distance, d_{off}, as seen in Fig. 6(c).

Because the front angle of the middle step is not 90° there is an asymmetry in d_{off} for the left- and right-moving steps, with d_{off} of the larger outgoing and incoming steps always being lower than that of the smaller outgoing and incoming steps by at least a factor of two, as shown in Fig. 6(c). This minimum ratio of offset distances corresponds to a front angle of 71.6°, very similar to the observed 75°. In addition, both offsets increase with increasing incoming step height sum, implying that the length of the middle step is related to the total relief between bounding planes. While d_{off} for the losing step is has a clear minimum ratio, it broadly does not correlate with the d_{off} for the winning step. In addition, for winning d_{off} above ≈50 microns, a second outgoing step is always observed. This implies that OPIs should have a single outgoing step that is the taller of the two incoming steps, but that the process that generates the middle step can also sometimes produce enough mixed mode I + III loading to nucleate a divergent step. That nucleation is stochastic in terms of both the polarity of step formed, and how far along or after the middle step it nucleates. In addition, the stresses generated during the formation of the middle step scale with the total incoming relief, and if the middle step is large enough this produces enough mixed mode loading to always nucleates a second outgoing step.

Overall, this reveals a framework for OPIs, where the larger incoming step wins, consuming the smaller incoming step and forming a middle step with an increased front angle of 71.6°. This increased front angle could be explained by the process that forms the middle step occurring more rapidly than

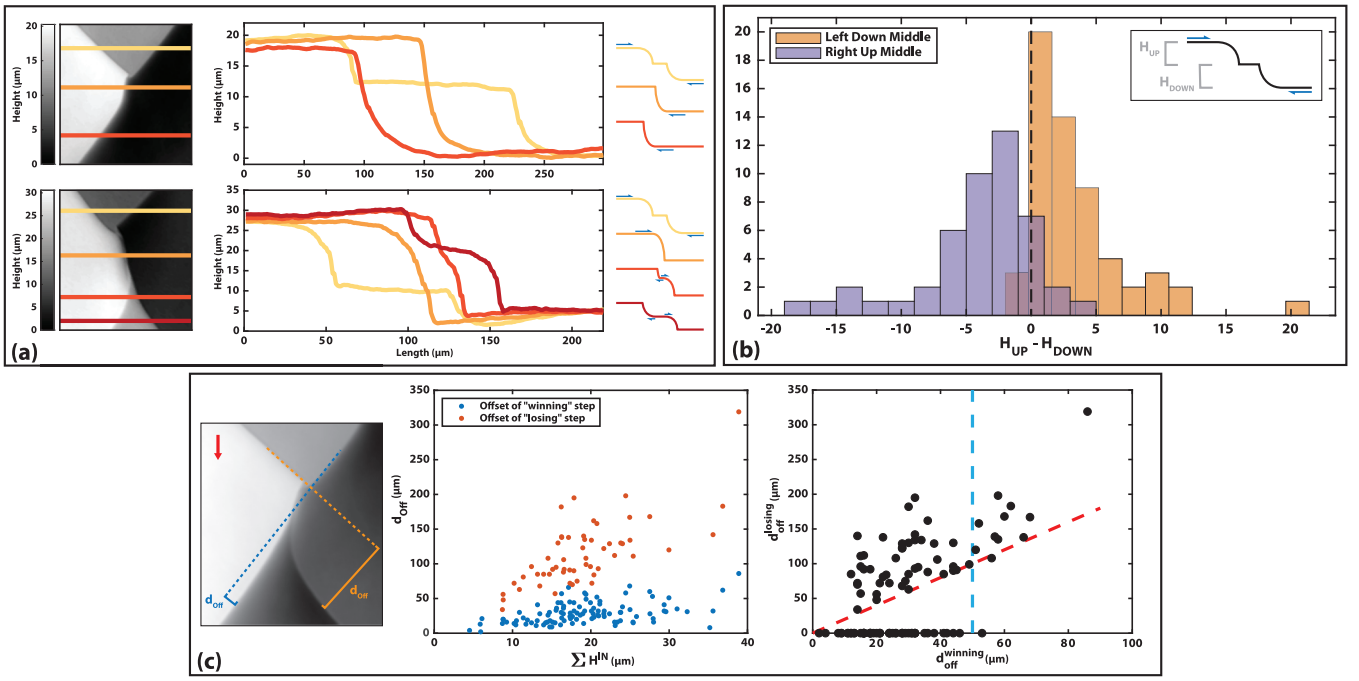

FIG. 6. An overview of opposite polarity interactions (OPIs). (a) Height maps (left), cross sections (middle), and schematics (right) for two typical examples of OPIs that result in one (top) or two (bottom) outgoing steps. Each height map is oriented so that the direction of crack propagation is from top to bottom. (b) Histogram of the resultant middle step drift and polarity as a function of the incoming height difference for OPIs. Each interaction has been mirrored so that the incoming steps look like the configuration shown in the inset so interactions can be directly compared. The histogram shows that the middle step retains the drift and polarity of the larger incoming step. (c) (left) Height map of a typical OPI with two outgoing steps. Each outgoing step is laterally offset from its original trajectory by an offset distance as indicated in the annotations. (middle) Offsets for the "winning" (step with the same drift and polarity as the middle step) and "losing" (nonwinning step) steps as a function of the total incoming relief. The losing steps always has a larger offset than the incoming steps, and the offset increases with the incoming relief. (right) Offset of the losing step as a function of the winning step. The losing offset is always at least a factor of two (angled red dashed line) times larger than the winning offset, but is otherwise stochastic. When the winning offset is greater than ≈50 microns (vertical blue dashed line) a losing step is always present.

the surrounding fracture. The larger the incoming relief, the longer the middle step, and the more stress that is generated by its formation. This process itself can sometimes produce enough of a twist to nucleate another outgoing step in the other direction, but its nucleation and polarity are stochastic.

VI. MERGING INTERACTIONS

The final class of interactions are merging interactions (MIs). MIs appear from above as sharp, hairpin like features, and occur when two nearby steps drifting in the same direction attract, accelerating towards one another, and eventually interacting as shown in Fig. 7(a). The step that trails in the direction of drift, which we refer to as the trailing step, is always the one that accelerates more, i.e., if both steps drift left, the rightmost step always accelerates to merge with the left.

MIs can occur for both same and opposite polarity step pairs, with each having slightly different morphology, as shown in Fig. 7(a). When the steps in an opposite polarity MI (OPMI) meet, they subtract like SPIs, such that if $|\Delta H^{IN}| \gg 0$ they produce a single step that spans the bounding planes, with a height of $\approx|\Delta H^{IN}|$ and the drift and polarity of the larger step. If $|\Delta H^{IN}| \approx 0$ the steps completely annihilate, similar to a V interaction without the residual hump. Also like SPIs, OPMIs are point-like interactions with the steps merging and the outgoing steps starting at a singular location. Same polarity MIs (SPMIs) are also defined by their bounding planes, with the resultant step being the sum of the incoming heights instead of the difference. As the two steps merge, the interaction is slightly elongated with the resultant trailing step slightly overriding the leading step (the nontrailing step), as seen in Fig. 7(a).

For every MI, the separation between the steps, s, decreases as a function of the distance from merging, d_m. For each interaction s scales as $\approx d_m^{1/2}$, as seen in Fig. 7(b). Elucidating the mechanism for this square-root power-law behavior would require both a detailed analysis of the perturbation to the stress field created by a single step, as well as an understanding of the interaction of defects confined to a one-dimensional crack front via the three-dimensional elastic bulk. However, noting that our system evolves quasistatically and assuming the dynamics are overdamped, one can deduce that the attractive forces between steps are long-range and decay as $1/s$.

VII. CONCLUSIONS

The average roughness of a brittle fracture surface is well described by a simple one-dimensional ballistic annihilation model, where steps are created randomly, propagate

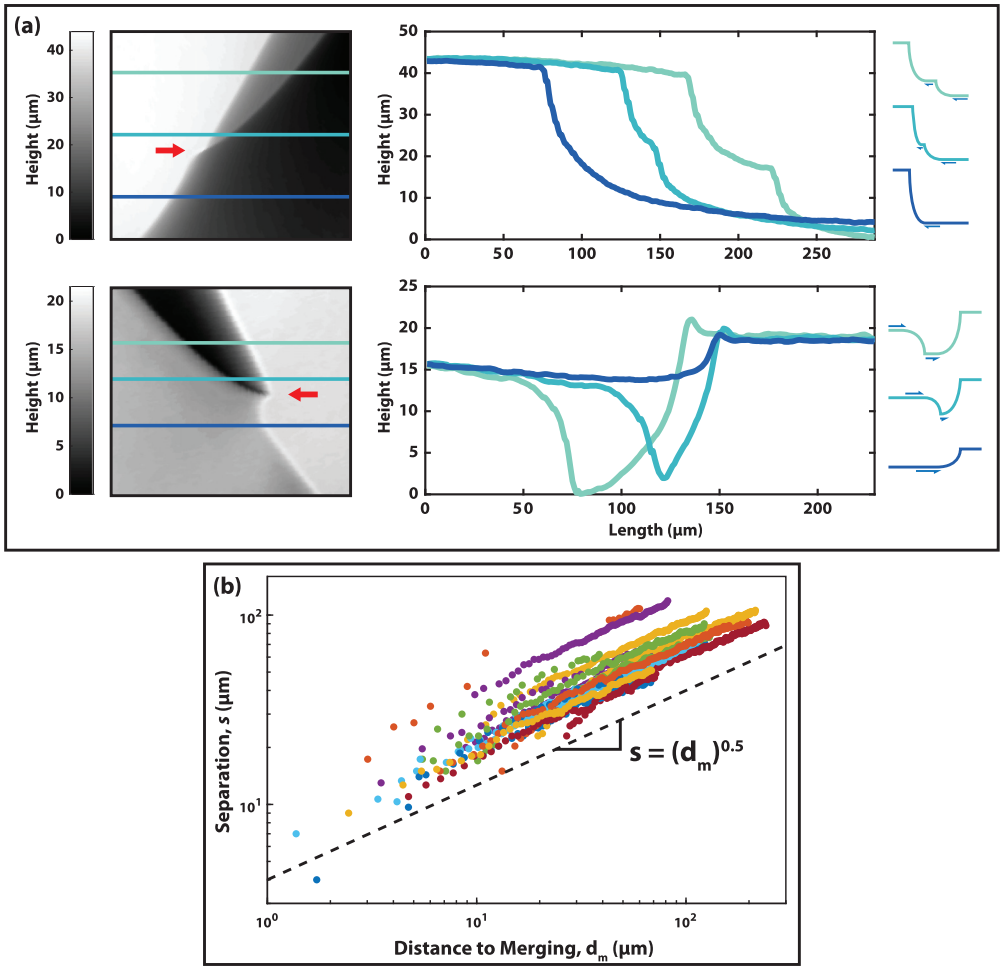

FIG. 7. An overview of merging interactions (MIs). (a) Height maps (left), cross sections (middle), and schematics (right) for two typical examples of MIs: (Top) a same polarity MI (SPMI), and (bottom) an opposite polarity MI (OPMI). Each height map is oriented so that the direction of crack propagation is from top to bottom. (b) Plot of the lateral separation distance s between merging steps as a function of distance from merging, d_m, for 19 measured MIs. The steps approach one another as the distance to the $1/2$ power (black-dashed line is a guide to the eye).

ballistically, and annihilate upon interaction with a constant probability [33]. However, through an exhaustive study of experimentally generated crack surfaces and a systematic analysis of hundreds of step interactions, we have identified the rules that govern step interactions on growing crack fronts and have shown that interactions are not random. Instead interactions can be constrained based on the geometry of the incoming steps and, thus, a single, constant probability for annihilation is insufficient. While the mean roughness for heterogeneous materials *is* well captured by a model that assumes random interactions, this may be due to the randomness of step formation in a complex medium. If there were a bias in the orientations of steps, for example, due to imposed boundary conditions as in some previous studies [11,27,28], these rules would predict a surface roughness not well captured by the mean-field model.

Step lines are a common feature of brittle fracture surfaces, and interactions with similar morphologies can be seen in previous studies in other materials [16,18,28,39,40]. In addition, crack surfaces of hydrogels with very high densities of heterogeneity [33] can resemble those observed in more complex brittle systems [41–45]. The mean-field model predicting crack roughness is based on ballistic annihilation kinetics and geometry, and thus, should be broadly applicable to brittle cracks in many materials. Since the rules described in this paper dictating step interactions have outcomes that are defined exclusively by their geometry, they should also apply broadly to any quasistatic brittle fracture.

Step interactions are dominated by the larger of the incoming steps. With the exception of OPMIs, for interactions that result in a single step, the outgoing step retains the morphology of the larger incoming step. This implies that steps generate a stress field that is a function of their height, which biases interactions in the direction of the larger incoming step. This is consistent with previous work showing that the front lag in the direction of crack propagation is proportional to the height of the step [18]. In addition, given the complex, three-dimensional nature of steps, this stress field is likely mixed mode, and plausibly explains why OPIs above a critical size always produce a second, divergent step.

Additionally, the only difference between OPIs and SPMIs is the orientation of one of the steps, and yet, the

interactions have markedly different morphologies. Combined with the asymmetry of the steps themselves, this points to some additional morphological complexity near the cusp of a step. One possible explanation is the presence of an undercutting fracture as described in previous work [14,17,18], but we have not observed this undercut directly. If an undercut indeed exists, it would likely be smaller than the resolution of our confocal microscope (<1 μm).

While step interactions follow rules that constrain potential outcomes, there are multiple possible results for statistically indistinguishable pairs of incoming steps. This randomness may be due to the heterogeneous background present within the gels, or alternatively, the apparent stochasticity may hint at an important three-dimensional aspect of the steps' shapes or their interactions. To determine this, a complete characterization of the three-dimensional dynamics of step interactions would be required.

ACKNOWLEDGMENTS

The authors would like to thank Simos Gerasimidis, Georgios Tzortzinis, Dmitry Garagash, Robert Viesca, Michael Moshe, Zhigang Suo, David Weitz, and Jim Rice for helpful discussions. This work was supported by the National Science Foundation through the Harvard Materials Research Science and Engineering Center Grant No. (DMR-1420570) and the Israel Science Foundation (Grant No. 2987/21).

[1] B. Lawn and T. R. Wilshaw, *Fracture of Brittle Solids* (Cambridge University Press, Cambridge, 1993).
[2] Y. W. Tsang and P. A. Witherspoon, J. Geophys. Res. **88**, 2359 (1983).
[3] A. Aydin, Mar. Pet. Geol. **17**, 797 (2000).
[4] A. Bunger and B. Lecampion, Four Critical Issues for Successful Hydraulic Fracturing Applications, *Rock Mechanics and Engineering*, edited by X.-T. Feng, Vol. 5 (CRC Press, Balkema, 2017), Chap. 16.
[5] E. E. Brodsky, J. J. Gilchrist, A. Sagy, and C. Collettini, Earth Planet. Sci. Lett. **302**, 185 (2011).
[6] E. E. Brodsky and J. Mori, Geophys. Res. Lett. **34**, L16309 (2007).
[7] T. Candela, F. Renard, J. Schmittbuhl, M. Bouchon, and E. E. Brodsky, Geophys. J. Int. **187**, 959 (2011).
[8] J. H. Dieterich and B. D. Kilgore, Pure Appl. Geophys. **143**, 283 (1994).
[9] J. A. Greenwood and J. B. P. Williamson, Proc. R. Soc. London, Ser. A: Math. Phys. Sci. **295**, 300 (1966).
[10] B. N. J. Persson, J. Chem. Phys. **115**, 3840 (2001).
[11] E. Sommer, Eng. Fract. Mech. **1**, 539 (1969).
[12] D. Hull, Int. J. Fract. **70**, 59 (1995).
[13] M. L. Cooke and D. D. Pollard, J. Geophys. Res. **101**, 3387 (1996).
[14] T. Baumberger, C. Caroli, D. Martina, and O. Ronsin, Phys. Rev. Lett. **100**, 178303 (2008).
[15] Y. Tanaka, K. Fukao, Y. Miyamoto, H. Nakazawa, and K. Sekimoto, J. Phys. Soc. Jpn. **65**, 2349 (1996).
[16] Y. Tanaka, K. Fukao, Y. Miyamoto, and K. Sekimoto, Europhys. Lett. **43**, 664 (1998).
[17] I. Kolvin, J. Fineberg, and M. Adda-Bedia, Phys. Rev. Lett. **119**, 215505 (2017).
[18] I. Kolvin, G. Cohen, and J. Fineberg, Nat. Mater. **17**, 140 (2018).
[19] R. V. Goldstein and N. M. Osipenko, Dokl. Phys. **57**, 281 (2012).
[20] D. Hull, Int. J. Fract. **62**, 119 (1993).
[21] O. Ronsin, C. Caroli, and T. Baumberger, Europhys. Lett. **105**, 34001 (2014).
[22] V. Lazarus, J.-B. Leblond, and S.-E. Mouchrif, J. Mech. Phys. Solids **49**, 1399 (2001).
[23] V. Lazarus, J.-B. Leblond, and S.-E. Mouchrif, J. Mech. Phys. Solids **49**, 1421 (2001).
[24] J.-B. Leblond, A. Karma, L. Ponson, and A. Vasudevan, J. Mech. Phys. Solids **126**, 187 (2019).
[25] C.-H. Chen, T. Cambonie, V. Lazarus, M. Nicoli, A. J. Pons, and A. Karma, Phys. Rev. Lett. **115**, 265503 (2015).
[26] A. J. Pons and A. Karma, Nature (London) **464**, 85 (2010).
[27] B. Lin, M. E. Mear, and K. Ravi-Chandar, Int. J. Fract. **165**, 175 (2010).
[28] K. H. Pham and K. Ravi-Chandar, Int. J. Fract. **199**, 105 (2016).
[29] K. H. Pham and K. Ravi-Chandar, Int. J. Fract. **206**, 229 (2017).
[30] D. Hull, *Fractography: Observing, Measuring and Interpreting Fracture Surface Topography* (Cambridge University Press, 1999).
[31] J.-B. Leblond and L. Ponson, C. R. Mec. **344**, 521 (2016).
[32] K. Ravi-Chandar and W. G. Knauss, Int. J. Fract. **26**, 65 (1984).
[33] W. Steinhardt and S. M. Rubinstein, Phys. Rev. Lett. **129**, 128001 (2022).
[34] Y. Elskens and H. L. Frisch, Phys. Rev. A **31**, 3812 (1985).
[35] S. Seiffert, Polym. Chem. **8**, 4472 (2017).
[36] See Supplemental Material at http://link.aps.org/supplemental/10.1103/PhysRevE.107.055003 for additional figures showing that both larger and smaller steps trend towards the steady state step height, and that the steady state height depends on the amount of cross-linker, but not the size of the step forming perturbation.
[37] J. Kim, G. Zhang, M. Shi, and Z. Suo, Science **374**, 212 (2021).
[38] Y. Wang, G. Nian, J. Kim, and Z. Suo, J. Mech. Phys. Solids **170**, 105099 (2023).
[39] Y. Tanaka, K. Fukao, and Y. Miyamoto, Eur. Phys. J. E: Soft Matter Biol. Phys. **3**, 395 (2000).
[40] A. N. Gent and C. T. R. Pulford, J. Mater. Sci. **19**, 3612 (1984).
[41] D. Bahat, *Tectonofractography* (Springer, Berlin, Heidelberg, 1991).
[42] A. M. Christensen and G. M. Hatch, J. Forensic Radiol. Imaging **18**, 37 (2019).
[43] T. Kimura, K. Ogawa, and M. Kamiya, Z. Rechtsmed. **79**, 301 (1977).
[44] M. Issa and A. Hammad, Cem. Concr. Res. **24**, 325 (1994).
[45] A. Carpinteri, B. Chiaia, and S. Invernizzi, Theor. Appl. Fract. Mech. **31**, 163 (1999).